A function for the thalamo-habenula projection

◆Ruey-Kuang Cheng[1], ◆Seetha Krishnan[2], Qian Lin[2], David G. C. Hildebrand[3, 4], Isaac H. Bianco[4], Caroline Kibat[5], Michelle Kee Zhi Ling[6] and *Suresh Jesuthasan[1,5, 6, 7]

[1]Lee Kong Chian School of Medicine, Nanyang Technological University, Singapore 636921.

[2]NUS Graduate School for Integrative Sciences and Engineering, 28 Medical Drive, National University of Singapore, Singapore 117456.

[3]Graduate Program in Neuroscience, Division of Medical Sciences, Graduate School of Arts and Sciences, Harvard University, Cambridge, Massachusetts 02138 United States of America.

[4]Department of Molecular and Cell Biology, Harvard University, Cambridge, Massachusetts 02138, United States of America.

[5]Neural Circuitry and Behavior Laboratory, Institute of Molecular and Cell Biology, Singapore 138673.

[6]Neuroscience and Behavioral Disorders Program, Duke-NUS Graduate Medical School, 8 College Road, Singapore 169857.

[7]Department of Physiology, National University of Singapore, Singapore 117597.

*Corresponding author: sureshj@ntu.edu.sg; +65 65869545

◆equal contribution

Abstract

The thalamus mediates diverse brain functions including arousal, perception and memory formation, and is characterized by widespread connectivity. One thalamus projection that is evolutionarily conserved is to the habenula, a regulator of broadly acting neuromodulators. The function of this projection is unknown, as the information transmitted has not been identified. By two-photon calcium imaging of larval zebrafish, we show that change in irradiance triggers dynamic responses in the habenula. Neuroanatomical tracing shows that the dorsal left habenula neuropil, which has the most prominent response to irradiance change and influences irradiance-dependent behavior and raphe response, is innervated by retinorecipient nuclei in the thalamus. Optogenetic stimulation of the thalamus triggers habenula activity, while lesion reduces light-evoked habenula activity. These data establish that the thalamus controls habenula activity following irradiance change, thereby suggesting that the thalamo-habenula projection provides a pathway for visual stimuli to affect neuromodulator release and behavior.

Introduction

The vertebrate thalamus receives information from virtually all regions of the brain including sensory systems, motor systems, basal ganglia and cerebellum, and in turn projects to multiple structures (Ward, 2013; Mitchell et al., 2014). It modulates the flow of sensory information to the cortex (Sherman and Guillery, 2002; Lee and Dan, 2012; Mitchell et al., 2014; Wimmer et al., 2015) and is considered a gateway to consciousness (Newman, 1995; Crick and Koch, 2003). Connectivity with the amygdala (Romanski and LeDoux, 1992) and nucleus accumbens (Cho et al., 2013) underlie roles in emotion and reward processing, while connectivity with the hippocampus is essential for memory formation (Aggleton et al., 2010) and navigation (Jankowski et al., 2013). A

47 less well known feature of thalamus connectivity is its innervation of the habenula
48 (Marburg, 1944; Cragg, 1961; Díaz and Puelles, 1992). The function of this projection is
49 unknown, as the information relayed from the thalamus to the habenula has not been
50 identified.

51 The habenula is an evolutionarily conserved structure (Stephenson-Jones et al.,
52 2012) that controls the release of broadly-acting neuromodulators such as serotonin,
53 dopamine, epinephrine and histamine (Wang and Aghajanian, 1977; Morley et al., 1985;
54 Jhou et al., 2009; Quina et al., 2014). As neuromodulators shape functional connectivity
55 in neural circuits (Getting, 1989; Marder, 2012; Bargmann and Marder, 2013), the
56 habenula can be viewed as a regulator of brain mode - defined as pattern of functional
57 connectivity (Getting, 1989). This role of the habenula is reflected by its involvement in
58 multiple behaviors, ranging from the control of fear (Agetsuma et al., 2010; Lee et al.,
59 2010; Zhang et al., 2016), to learning (Matsumoto and Hikosaka, 2007; 2009; Amo et al.,
60 2014), addiction (Fowler et al., 2011), sleep (references), and performance under stress
61 (Thornton and Davies, 1991) .

62 The habenula regulates neuromodulators based on inputs reflecting reward value,
63 internal state and sensory stimuli. The entopeduncular nucleus, or internal segment of
64 the globus pallidus, provides excitatory input in response to negative reward (Hong and
65 Hikosaka, 2008). Internal states such as circadian clock, may be conveyed from the
66 hypothalamus, from example by hypocretin-secreting neurons (Appelbaum et al., 2009).
67 Odor-evoked activity in the habenula, which has been documented in the zebrafish
68 (Krishnan et al., 2014), is mediated by a direct input from the olfactory bulb (Miyasaka et
69 al., 2009). Light-evoked activity has been detected in the habenula in rat (Zhao and
70 Rusak, 2005), pigeon (Semm and Demaine, 1984) and zebrafish (Dreosti et al., 2014).
71 Reduction in irradiance has also been shown to affect the habenula (Portugues et al.,

2014; Bianco and Engert, 2015). How changes in irradiance affect the habenula is unclear.

The thalamus receives input from all sensory systems, except the olfactory system. It is thus possible that the pathway from the thalamus to the habenula functions to control habenula activity in response to change in irradiance. Here we provide evidence for this hypothesis. In doing so, this paper identifies one function of the thalamus-habenula projection.

Results

The habenula displays dynamic response to irradiance change

The zebrafish habenula consists of neurons surrounding neuropils that are innervated by afferent neurons (Hendricks and Jesuthasan, 2007; Miyasaka et al., 2009; Amo et al., 2014). To identify the pathways by which change in irradiance influences the habenula, we first characterized habenula activity evoked by these changes. Two-photon imaging was performed on a transgenic zebrafish line expressing the calcium indicator GCaMP3 in the habenula (Krishnan et al., 2014) (Figure 1A). Resonant-scanning, combined with piezo-driven focusing, was used to record the activity of cells at multiple focal planes throughout the habenula (Figure 1B, C). With a step size of 10 μm, so that each cell would be sampled only once, most of the habenula could be covered with 5 planes at a rate of 1 Hz. Habenula activity was monitored as the larva was exposed to discrete pulses of blue light. Pixel-wise analysis in one fish indicates that evoked activity – both transient and sustained - occurred throughout the habenula in response to both increase and decrease in irradiance (Figure 1D, E). The spatio-temporal pattern of activity was reproducible across several cycles, as shown by the trajectory of the system through state space (Figure 1F).

To assess if responses were reproducible across multiple fish, we imaged the habenula in 6 fish. Habenula neurons were segmented (Figure 2A-C; total of 4986 cells, with an average of 831 ± 53 cells (95% CI) per fish) and their activity was clustered by *k*-means. Cluster centers were classified by response type. Transient and sustained responses to increase and decrease in irradiance could be reliably evoked (Figure 2D-F). The percentage of responding cells per fish (±95% CI) were ON: 30.98 ± 9.94%; OFF: 19.03 ± 3.93%; Inhibitory: 7.93 ± 3.50%. Correlating the cells corresponding to the different response types revealed that, in general, neurons that were excited by an increase of irradiance did not fire to a decrease (Figure 2G, H). Some neurons that were inhibited by light did, however, show a response at light offset (Figure 2F, blue trace; see also Figure 1E, red trace). These observations confirm that the activity of zebrafish habenula neurons is affected by change in irradiance, and that in addition to excitation there is inhibition by light, as well as excitation to loss of light.

Activity occurs prominently in the dorsal left neuropil

To obtain a more detailed view of light evoked activity, we used higher speed widefield microscopy. With imaging at 20 Hz, responses was detected in multiple regions of the habenula at the onset of the LED used to induce fluorescence of the reporter (Movie 1). One region with a reproducible increase in fluorescence was the dorsal left neuropil (Figure 3A-C; n = 6 fish). The calcium indicator R-GECO (Zhao et al., 2011), which has a faster rise time than GCaMP3 (approx 10 msec half rise time (Akerboom et al., 2013)) and is more sensitive (Walker et al., 2013), also showed a reproducible strong rise in the dorsal left neuropil (Movie 2; Figure 3D-H; n = 3 fish). As the calcium indicator is expressed in habenula neurons in both these lines, this neuropil response probably occurs in dendrites, implying that at least some information about irradiance change is provided by afferents to the dorsal left neuropil.

To further explore this, we performed imaging in the *Tg(elavl3:GCaMP6f)* line, which has broad expression of a calcium-reporter, and thus likely also in afferent neurons. A prominent increase in fluorescence was detected in neuropil of the dorsal left habenula (Movie 3; Figure 3I-K). This was seen in all fish imaged (n = 3) and may reflect activity in terminals of afferent neurons. In addition to the asymmetric habenula neuropil response, bilateral increase was seen more posteriorly, within the thalamic/pretectal area (Fig. 3J). This latter symmetry argues against the habenula response being a result of asymmetric expression of the reporter. Rather, the pattern of increase in the habenula suggests that information regarding increase in irradiance is conveyed asymmetrically to the left dorsal neuropil.

We asked what role activation of the dorsal left neuropil might have. Larval zebrafish show a strong preference for light over darkness (Steenbergen et al., 2011), which appears to involve the dorsal raphe (Cheng et al., 2016). Lesioning the dorsal neuropil of the left habenula with the two-photon laser (Supplemental Figure 1A-C) led to a reduction in this preference (Supplemental Figure 1D-F; $p = 0.0086$ Mann-Whitney's U test; effect size $r = 0.413$). This manipulation also led to an alteration of raphe response to change in irradiance (Supplemental Figure 1G-K). Instead of the inhibition to increase in irradiance in the anterior raphe, there was an excitation. These observations indicate that the dorsal left neuropil influences irradiance-dependent neuromodulator release and behavior.

The thalamus provides a source of input to the dorsal left neuropil

The entopeduncular nucleus (EN) is the major source of habenula afferents in teleosts (Yañez and Anadon, 1994), including zebrafish (Amo et al., 2014). This nucleus is labeled in the *Et(sqKR11)* line (Lee et al., 2010), providing a simple way of visualizing

EN afferents to the habenula. Some labeled fibers were detected in the dorsal left neuropil, indicating that the EN does provide innervation to this region of the habenula (Figure 4A). To test for additional input sources, the lipophilic tracer DiD was injected into the dorsal left neuropil (n = 6 fish). In all cases, neurons in the dorsal left habenula (which extend dendrites into the neuropil), the parapineal, and a thalamic nucleus located ventrally to both habenula (Figure 4B-D) were labelled. DiD label was not detected in any other regions of the brain, and only rarely in the entopeduncular nucleus (Figure 4C), suggesting that the thalamus is the major source of input to the dorsal left neuropil. The label in the thalamus cannot represent anterograde label from the habenula, as tracing of projections from the habenula by expressing fluorescent proteins specifically in the habenula does not result in a projection to the thalamus (Movie 4). Moreover, the labeling of cell bodies in the thalamus (Figure 4D inset, E) indicates that this is likely to be a retrograde label. The neuropil of this thalamic nucleus contains terminals of retinal ganglion cells, as shown by DiI injection into the retina (Figure 4E, F). Based on the location of these terminals relative to the optic tract, these terminals make up AF2 and AF4 (Easter and Nicola, 1996; Robles et al., 2014). Thus, the habenula neuropil with the initial response to light is innervated by thalamic nuclei that receive retinal input.

The habenula may receive glutamatergic and GABAergic input from the thalamus

Light caused both excitation and inhibition in zebrafish habenula neurons, implying that there may be excitatory and inhibitory afferents. Using an antibody to vGlut1/2, glutamatergic pre-synapses were detected in all neuropils of the habenula, including the dorsal left neuropil (Figure 4G), indicating the existence of excitatory afferents. GAD65/67 labeled puncta could also be detected in the dorsal left neuropil (Figure 4H). Label was seen also in other neuropils, while in the lateral regions, corresponding to the

ventral habenula, streaks were detected adjacent to cell bodies. These labels were not located within habenula neurons, as they did not co-localize with cytoplasmic label provided by GCaMP3, nor did they fill the cytoplasm, implying that these puncta and streaks must reside in habenula afferents (i.e. axon terminals). Labeled cell bodies were seen below the level of the habenula [see Movie 5]. Consistent with this, inhibitory neurons could be detected in the dorsal thalamus using the transgenic line *Tg(gad1b:RFP, vGlut2a:GAL4, UAS:eGFP)* (Satou et al., 2013) (Figure 4I, J; Movie 6). No label was seen in the entopeduncular nucleus, which has previously been shown to be glutamatergic (Amo et al., 2014). These observations confirm that the thalamus contains both GABAergic and glutamatergic neurons, as described previously (Mueller, 2012), which may mediate light-evoked excitation and inhibition of habenula neurons.

Irradiance change evokes activity in thalamus neurons

If the thalamus provides afferents mediating illumination-dependent information to the habenula, there should be responses to increase and decrease of illumination in thalamic neurons. To test this, calcium imaging was carried out using a driver line with GAL4 expression in the thalamic neurons that innervate that habenula (Figure 5A, B). A response to increase and decrease in irradiance was detected in scattered cells in the anterior thalamus (Figure 5C-I) in all fish imaged (n = 5, Figure 5 J,K). The response to increase in irradiance was more prominent in the dorsal region of the neuropil (cyan pixels; Figure 5C-E, 5J), whereas response to decrease (magenta pixels) was more prominent ventrally (Figure 5K). Terminals of neurons within the habenula also showed a response (Figure 5L-O). These observations indicate that change in irradiance leads to activity in thalamic neurons innervating the habenula, with different subsets responding to increase versus decrease.

Optogenetic stimulation of the thalamus drives habenula activity

To test the ability of thalamic neurons to drive activity in the habenula, we used optogenetics. Channelrhodopsin-2 (ChR2) was expressed in thalamic neurons using the *s1020tGAL4* driver (Figure 6A). Experiments were carried out on fish lacking eyes, to prevent a response to visual stimulation. Short pulses of blue light reproducibly caused an increase in fluorescence of GCaMP6f in habenula neurons of fish with expression of ChR2 in the thalamus (Figure 6B-E, G). A small response was seen in fish without ChR2 expression (Fig. 6F), however, implying that some habenula response may be due to deep brain photoreceptors (Fernandes et al., 2013). The larger response in fish with ChR2 expression suggests that neural activity in thalamic neurons can elicit a response in the habenula.

Thalamic lesion inhibits habenula response to illumination change

To test the role of the thalamus pathway in light-evoked activity in the habenula, we lesioned the thalamus neuropil with a two-photon laser. The laser was targeted to the region of AF4 that showed excitation to light ON (Figure 7A-C). This manipulation is expected to damage fibers innervating this neuropil (Semmelhack et al., 2014). Following lesion, there was a reduction of evoked activity in the habenula (Figure 7D-F, I). There was some variability in the effect, possibly reflecting the limitations of this technique in enabling consistent ablation of the entire neuropil. Lesioning other targets of retinal ganglion cell axons did not lead to a loss of light-evoked activity (Figure 7G, I). These observations support the hypothesis that a pathway involving the thalamic neuropil AF4 has a role in light-evoked activity in the habenula.

Discussion

This paper identifies one function of the projection from the thalamus to the habenula. By calcium imaging, we found that increase and decrease in irradiance

causes activity throughout the habenula. A strong increase in the fluorescence of calcium reporters was detected in the neuropil of the dorsal left habenula. Although calcium indicators are only a proxy for neural activity, i.e. reflecting the opening of voltage sensitive calcium channels, and have slow dynamics, they can indicate the number of spikes (Chen et al., 2013). The strong fluorescence in the dorsal left neuropil may thus reflect relatively high spiking rate of afferents following change in irradiance. These afferents appear to derive primarily from the thalamus. Lipophilic tracing and labeling of thalamic neurons with the *GAL4s1020t* driver demonstrate that the thalamus directly innervates the zebrafish habenula. Optogenetic stimulation of the thalamus led to activity in the habenula, while lesion inhibited light-evoked activity. Thus, by calcium imaging, anatomical tracing and manipulation, our data demonstrates that innervation from the thalamus enables habenula responses to irradiance change.

The region of the thalamus mediating activity in the habenula can be functionally separated into two domains, based on the response to light – excitation to light OFF in the ventral regions and excitation to light ON more dorsally. The neuropil of the thalamus contains two previously defined targets of retinal ganglion cells - AF2 and AF4 (Burrill and Easter, 1994), and would thus correspond to first-order nuclei. AF4 is innervated predominantly by M3 and M4 retinal ganglion cells (Robles et al., 2014), which extend their dendritic tree into the proximal layer of the inner plexiform layer and are considered ON neurons. AF2 is innervated by B1 retinal ganglion cells that have dendrites in the distal layer (Robles et al., 2014), and these may account for the OFF responses in the thalamus and habenula. The distinct domains suggest that the habenula is innervated by two retino-recipient thalamic nuclei; these nuclei may also receive input from non-retinal sources, but this remains to be investigated.

Light is a potent regulator of brain function – it can affect mood (Vandewalle et al.,

2010), alertness (Badia et al., 1991), cognitive ability (LeGates et al., 2012) and movement (Aschoff, 1960; Burgess and Granato, 2007). These phenomena are sensitive to irradiance, not image formation, and are mediated by a number of sensors including intrinsically-sensitive retinal ganglion cells (Hattar et al., 2003), and deep brain detectors (Fernandes et al., 2012; Kokel et al., 2013). The ability of light to affect normal movement patterns (Burgess et al., 2010) or to disrupt mood and cognition (LeGates et al., 2012) involves neuromodulators such as serotonin, and changing irradiance affects activity in the dorsal raphe (Fite et al., 2005; Cheng et al., 2016). Based on the data here, and the well-established roles of the habenula in regulating neuromodulators, we suggest that some of these effects of light may be mediated by the thalamic projection to the habenula.

Materials and Methods

Fish lines

Experiments were performed in accordance with guidelines issued by the Institutional Animal Care and Use Committee of the Biological Resource Centre at Biopolis, Singapore. Zebrafish (*Danio rerio*) lines used for this study were: *Tg(UAS:GCaMP6s)sq202*, SqKR11Et, *GAL4s1011t*, *GAL4s1020t, Tg(UAS-R-GECO),* Tg(UAS:GCaMP3)sq200, *Tg(elavl3:GCaMP6f)a12200*, *Tg(UAS:ChR2-eYFP)*(Arrenberg et al., 2009) and AB wildtype.

Tg(elavl3:GCaMP6f)a12200 was generated by PCR amplification of the GCaMP6f open reading frame (Addgene plasmid 40755 (Chen et al., 2013)) with forward primer ataACTAGTgccaccATGGGTTCTCATCATCAT and reverse ataCCGCGGcTCACTTCGCTGTCATCATTTGTAC (restriction site and coding sequences are in upper case). This fragment was cloned into a plasmid with Tol2 arms

flanking an upstream attR1-R2 cassette and the insertion site using restriction enzymes SpeI and SacII. Previously described *elavl3* (*HuC*) *cis*-regulatory elements (Higashijima et al., 2003) were placed upstream via LR recombination (Invitrogen) with an attL flanked *elavl3* entry clone. The resulting plasmid was then co-injected into 1-cell stage embryos at a concentration of 30 ng/µL with Tol2 transposase mRNA at a concentration of 30 ng/µL. A single founder was selected based on high and spatially broad expression. Outcrossing this founder generated 50% GCaMP6f-positive embryos, which were selected to establish the line.

Imaging

Zebrafish larvae (aged 5 - 10 dpf) were anaesthetized in mivacurium and embedded in low-melting temperature agarose (1.2-2.0 % in E3) in a glass-bottom dish (Mat Tek). They were imaged on a Nikon two-photon microscope (A1RMP), attached to a fixed stage upright microscope, using a 25x water immersion objective (NA = 1.1). The femtosecond laser (Coherent Vision II) was tuned to 920 nm for GCaMP imaging. Stacks were collected in resonant-scanning mode with a 525/50 nm bandpass emission filter and with 8x pixel averaging; single-plane images were collected in galvano-scanning mode with 2x pixel averaging. The sample size was based on (Dreosti et al., 2014).

Light stimuli were generated by 5 mm blue LEDs (458 nm peak emission). They were powered by a 5 V TTL signal from a control computer and synchronized with image capture using a National Instruments DAQ board, controlled by the Nikon Elements software. Light intensity at the sample was 0.13 mW/cm^2.

For widefield microscopy, excitation was provided by LEDs (Cairn OptoLED) at 470 nm. Images were captured on a Zeiss Axio Examiner with a 40x water immersion objective, using an Evolve camera (Photometrics) or a Flash4 camera (Hamamatsu).

After background subtraction, ratio images were obtained by dividing each frame against the first frame of this time-stack using Fiji. A mask, created with Fiji, was used to isolate the fluorescent structures. Movie 2 was made using the ratio command in MetaMorph, after background subtraction.

Data analysis

Data Preprocessing: Raw images obtained were first registered to correct for any vertical/horizontal movement artifacts using cross correlation. In case of high speed data using a resonant scanner, a median filter of size 3 was applied to remove noise. A darker region outside the region of interest was chosen as the background and subtracted from the image to remove any background noise. Non linear trends in the data were detrended using polynomials of order 2-5. Data was then normalized into Z-scores by subtracting the overall mean and dividing by the standard deviation. A rolling window average was then used to smooth noisy traces where necessary.

Analysis of Habenula and Thalamus: The Thunder platform (Freeman et al., 2014) was used for fast pixel based clustering and factorization. Principal Component Analysis (PCA) was used to obtain a low dimensional representation. The number of principal components was identified based on the total variance explained. *K-means* clustering was performed to identify pixels with similar responses profiles. The number of clusters (*k*) was chosen such that cluster members were highly correlated with the cluster centroid and to each other after multiple iterations. Details for different data sets are given below.

Figure 1D-E shows the temporal and spatial distribution of responses to change in irradiance and is not intended for cell segmentation. Since pixel based analysis are sensitive to noise, images were first run through a median filter of kernel size 5 and time

316 traces were detrended and smoothed before clustering was performed. The number of
317 clusters were chosen to reveal as many stimulus related clusters as possible, until there
318 was little change in the number and types of stimulus related clusters and increase in
319 noise related clusters. Noise clusters were then removed from the spatial and temporal
320 plots for clarity. After multiple runs, k-means was performed for *k*=10. 6 clusters were
321 light related and are shown in Figure 1D-E, 4 noisy clusters were removed. Similarly, for
322 Figures 5C-I, *k-means* was run on 6 focal planes obtained from the thalamus with *k*=8, 4
323 light related clusters are plotted in Figure 5I, 4 were removed.

324 For Figures 2D-F, *k-means* was performed from cells segmented by a semi
325 automated algorithm (see below). The purpose is to show heterogeneity of temporal
326 responses to changes in irradiance, accurately classify cells into ON, OFF and Inhibitory
327 responses and perform correlation between them. Analysis was done on traces from
328 4986 cells from 6 fish. Traces were detrended, smoothed and normalized to z-scores
329 using baseline as the time before the first blue light. Traces that did not reach a Z-score
330 of 2 during the period of irradiance change were classified as not having an evoked
331 response and not included in the clustering analysis. 2456 of 4986 cells were thus
332 removed. *K-means* was first run with an arbitrary *k* = 60. This generated a wide range of
333 clusters capturing the temporal heterogeneity of the responses. The clusters were then
334 divided into ON, OFF, Inhibitory and No response. Neurons belonging to each cluster
335 were correlated among each other and to the cluster centroid. Neurons with low
336 correlation (<0.6) were inspected, if they had no evoked response, they were discarded.
337 If they had an evoked response, they were correlated with other clusters and assigned to
338 one with the highest correlation. 138 such cells were reclassified.

339 For data following AF4/AF9/AF7 lesion (Figure 7), *k-means* was performed to
340 differentiate responses between the controls and the lesion. Hence, number of clusters

were chosen such that cluster centroids adequately differentiated responses before and after lesion. Cluster centroids not responding to light were also plotted here.

Terminals of thalamic afferents in neuropils of the habenula were isolated pixels in the image that showed increases in calcium to changes in irradiance. For Figure 5 L-O, recordings from two fish were registered and averaged. The images were then thresholded to find pixels with high standard deviation and those corresponding to ON and OFF were plotted.

For images obtained with widefield microscopy, which included out-of-focus information, non-negative matrix factorisation (NMF) was used for accurate source separation and identifying temporal differences in regions of the habenula. NMF factorizes a non-negative matrix V, into two non-negative matrices W and H (Maruyama et al., 2014). For Figure 3G-H, 4 recordings from the same fish were registered (using TurboReg in ImageJ) and NMF was run on a dataset formed by averaging the recordings and filtering the resulting images with a median filter of window 5. The algorithm was run multiple times with different number of components *k*, ensuring convergence of at least 0.01 in H. Finally, *k*=6 was selected for its accuracy in picking the different temporal profiles when compared to manual inspection.

The scripts used for analysis are provided at http://dx.doi.org/10.5061/dryad.q0171.

Segmentation of Region of interest (ROI): Each stack was scaled 2x in imageJ, then maximally projected to a single image, which was then subjected to a minimum filter and unsharp mask to sharpen the boundary of cells. ROIs were identified using the “find maxima…” command, as a way to localize regional darkest point as the center of each ROI. The boundary of the ROI was outlined by “analyze particle…” that connects bright pixels into mosaic-like tessellated plane, encircling each darkest point. Each ROI was

then numbered sequentially using the ImageJ ROI Manager and mapped back to the original despeckled image stack. Manual segmentation was done here to delete extraneous ROIs outside the habenula and to encircle cells that were not detected by the algorithm (<10% of total ROIs). In the last step, "Set measurements…" and "measure" in ImageJ provided the mean fluorescence value of all pixels within each ROI across the entire image stack and the x-y coordinates of each ROI. Time-lapse series in which z drifting occurred were excluded, as in this case ROIs could not be defined.

Ratio images: Following background subtraction, a ratio of each plane relative to the first plane was obtained using FIJI. A median filter (radius = 1.0 pixels) and a mask was then applied.

Neural tracing

DiD (Life Technologies) was dissolved in 50 µl ethanol to make a saturated solution. This was heated to 55˚C for 5 minutes prior to injection into the fish that had been fixed in 4% paraformaldehyde. Fish were mounted in 1.2% low melting temperature agarose dissolved in PBS. The dye was pressure injected into the habenula under a compound microscope (Leica DM LFS), using a 20X water immersion objective. For labeling the retina, a saturated solution of DiI in chloroform was used. Injections were carried out under a stereo microscope (Zeiss Stemi 2000). After injections, fish were stored at 4˚C overnight to allow tracing, and then imaged with a 40x water immersion objective on a Zeiss LSM 710 confocal microscope.

Antibody label

Larvae were fixed in 4% para-formaldehyde/PBS overnight at 4˚C. They were then rinsed in PBS. The brains were dissected out, and permeabalized using 1% BSA

(fraction V; Sigma), 0.1% DMSO and 0.1% Triton X-100. The antibodies used here, anti-vGlut1/2 (Synaptic Systems 135503, RRID:AB_1279466; 1:100) and anti-GAD65/67 (Abcam ab11070, RRID:AB_297722; 1:500), have previously been used in zebrafish (Wyart et al., 2009; Lee et al., 2010). The brains were incubated in the primary antibody overnight, rinsed several times in PBS, then incubated in secondary antibody (Alexa 488 goat anti-rabbit; 1:1000). After washing, these were mounted in 1.2% agarose/PBS. Imaging was carried out using a Zeiss LSM 510 laser scanning confocal microscope, with a 40x water immersion objective.

Optogenetic stimulation

5 dpf *Tg(s1020GAL4, UAS:ChR2-eYFP, elavl3:GCaMP6f)* larvae were used. The eyes were removed using fine tungsten needles in fish that were anesthetized with MS222. This procedure was carried out in Ringers saline. Fish were then mounted in 1.2% agarose in Ringers saline, and imaged using two-photon microscopy as described above, at 1 Hz. Optical stimulation was carried out using a 50 µm fiber optic probe (Doric Lenses), placed approximately 20 µm from the thalamus. The 465 nm LED (Doric) was driven with a current of 900 mA, 30 seconds after the start of imaging. 10 pulses were provided, with a pulse duration of 25 milliseconds and a frequency between 1 and 8 Hz. Each fish was exposed to at least 3 pulse trains. For Figure 6B-C, the average of the first 29 frames was used as a reference. The ratio of all frames relative to this reference was obtained using FIJI. The analysis to generate Figure 6G was blind to the genotype.

Laser ablation

Tg(Elavl3:GCaMP6f) larvae were anaesthetized and then mounted in 2% low-melting temperature agarose. Lesions were created with the femto-second laser tuned to 960 nm and fixed on a single point. Several pulses, each lasting 100 - 500 msec, were used. Lesioning was monitored by time-lapse imaging before and after each pulse, and

was terminated when there was a localized increase in GCaMP6f fluorescence. Sample size was chosen based on (Aizenberg and Schuman, 2011). Animals with bleeding in the brain after lesioning, due to bursting of a blood vessel in AF4, were discarded.

Behavioural Assay

The chamber for the light/dark assay has been described previously (Cheng et al., 2016). Control fish were mock-lesioned, i.e. subject to the same anaesthetic (MS222) and mounted in agarose for the same duration as lesioned fish. Fish were observed in the chamber for 10 minutes, by imaging at 15 Hz under infra-red illumination.

Acknowledgements

This work was funded by core funding from the Institute of Molecular and Cell Biology and a grant from the Ministry of Education, Singapore. SK and QL were supported by fellowships from the National University of Singapore. DGCH was supported by NIH grant 5T32HL007901. We thank Claire Wyart for providing the *UAS:ChR2* transgenic line.

Author contributions

Experiments were designed by CRK, QL and SJ. CRK carried out two-photon imaging. SK developed software and analyzed imaging data. CK performed antibody label and generated the *UAS:GCaMP6s* line. MKZL performed the behavior assay, using fish lesioned by QL. DGCH and IHB generated the *elavl3:GCaMP6f* transgenic line. SJ performed wide-field imaging, analysis, dye tracing, optogenetic manipulation and wrote the manuscript.

References

Agetsuma M, Aizawa H, Aoki T, Nakayama R, Takahoko M, Goto M, Sassa T, Amo R,

436 Shiraki T, Kawakami K, Hosoya T, Higashijima S-I, Okamoto H (2010) The habenula
437 is crucial for experience-dependent modification of fear responses in zebrafish. Nat
438 Neurosci 13:1354–1356.

439 Aggleton JP, O'Mara SM, Vann SD, Wright NF, Tsanov M, Erichsen JT (2010)
440 Hippocampal-anterior thalamic pathways for memory: uncovering a network of direct
441 and indirect actions. European Journal of Neuroscience 31:2292–2307.

442 Aizenberg M, Schuman EM (2011) Cerebellar-Dependent Learning in Larval Zebrafish. J
443 Neurosci 31:8708–8712.

444 Akerboom J et al. (2013) Genetically encoded calcium indicators for multi-color neural
445 activity imaging and combination with optogenetics. Front Mol Neurosci 6:2.

446 Amo R et al. (2014) The habenulo-raphe serotonergic circuit encodes an aversive
447 expectation value essential for adaptive active avoidance of danger. Neuron
448 84:1034–1048.

449 Appelbaum L, Wang GX, Maro GS, Mori R, Tovin A, Marin W, Yokogawa T, Kawakami K,
450 Smith SJ, Gothilf Y, Mignot E, Mourrain P (2009) Sleep-wake regulation and
451 hypocretin-melatonin interaction in zebrafish. Proceedings of the National Academy
452 of Sciences 106:21942–21947.

453 Arrenberg A, Arrenberg AB, Del Bene F, Del Bene F, Baier H, Baier H (2009) Optical
454 control of zebrafish behavior with halorhodopsin. Proceedings of the National
455 Academy of Sciences 106:17968–17973.

456 Aschoff J (1960) Exogenous and endogenous components in circadian rhythms. Cold
457 Spring Harb Symp Quant Biol 25:11–28.

458 Badia P, Myers B, Boecker M, Culpepper J, Harsh JR (1991) Bright light effects on body
459 temperature, alertness, EEG and behavior. Physiol Behav 50:583–588.

460 Bargmann CI, Marder E (2013) From the connectome to brain function. Nat Methods
461 10:483–490.

462 Bianco IH, Engert F (2015) Visuomotor transformations underlying hunting behavior in
463 zebrafish. Curr Biol 25:831–846.

464 Burgess HA, Granato M (2007) Modulation of locomotor activity in larval zebrafish during
465 light adaptation. J Exp Biol 210:2526–2539.

466 Burgess HA, Schoch H, Granato M (2010) Distinct retinal pathways drive spatial
467 orientation behaviors in zebrafish navigation. Curr Biol 20:381–386.

468 Burrill JD, Easter SS (1994) Development of the retinofugal projections in the embryonic
469 and larval zebrafish (Brachydanio rerio). J Comp Neurol 346:583–600.

470 Chen T-W, Wardill TJ, Sun Y, Pulver SR, Renninger SL, Baohan A, Schreiter ER, Kerr
471 RA, Orger MB, Jayaraman V, Looger LL, Svoboda K, Kim DS (2013) Ultrasensitive
472 fluorescent proteins for imaging neuronal activity. Nature 499:295–300.

473 Cheng R-K, Krishnan S, Jesuthasan S (2016) Activation and inhibition of tph2
474 serotonergic neurons operate in tandem to influence larval zebrafish preference for
475 light over darkness. Sci Rep 6:20788.

476 Cho YT, Fromm S, Guyer AE, Detloff A, Pine DS, Fudge JL, Ernst M (2013) Nucleus
477 accumbens, thalamus and insula connectivity during incentive anticipation in typical
478 adults and adolescents. Neuroimage 66:508–521.

479 Cragg BG (1961) The connections of the habenula in the rabbit. Exp Neurol 3:388–409.

480 Crick F, Koch C (2003) A framework for consciousness. Nat Neurosci 6:119–126.

481 Díaz C, Puelles L (1992) Afferent connections of the habenular complex in the lizard
482 Gallotia galloti. Brain Behav Evol.

483 Dreosti E, Vendrell-Llopis N, Carl M, Yaksi E, Wilson SW (2014) Left-right asymmetry is
484 required for the habenulae to respond to both visual and olfactory stimuli. Curr Biol
485 24:440–445.

486 Easter SS, Nicola GN (1996) The development of vision in the zebrafish (Danio rerio).
487 Dev Biol 180:646–663.

488 Fernandes AM, Fero K, Arrenberg AB, Bergeron SA, Driever W, Burgess HA (2012)
489 Deep brain photoreceptors control light-seeking behavior in zebrafish larvae. Curr
490 Biol 22:2042–2047.

491 Fernandes AM, Fero K, Driever W, Burgess HA (2013) Enlightening the brain: Linking
492 deep brain photoreception with behavior and physiology. Bioessays 35:775–779.

493 Fite KV, Wu PS, Bellemer A (2005) Photostimulation alters c-Fos expression in the
494 dorsal raphe nucleus. Brain Res 1031:245–252.

495 Fowler CD, Lu Q, Johnson PM, Marks MJ, Kenny PJ (2011) Habenular α5 nicotinic
496 receptor subunit signalling controls nicotine intake. Nature 471:597–601.

497 Getting PA (1989) Emerging principles governing the operation of neural networks.
498 Annual Review of Neuroscience 12:185–204.

499 Hattar S, Lucas RJ, Mrosovsky N, Thompson S, Douglas RH, Hankins MW, Lem J, Biel

M, Hofmann F, Foster RG, Yau K-W (2003) Melanopsin and rod-cone photoreceptive systems account for all major accessory visual functions in mice. Nature 424:76–81.

Hendricks M, Jesuthasan S (2007) Asymmetric innervation of the habenula in zebrafish. J Comp Neurol 502:611–619.

Higashijima S-I, Masino MA, Mandel G, Fetcho JR (2003) Imaging neuronal activity during zebrafish behavior with a genetically encoded calcium indicator. J Neurophysiol 90:3986–3997.

Hong S, Hikosaka O (2008) The globus pallidus sends reward-related signals to the lateral habenula. Neuron 60:720–729.

Jankowski MM, Ronnqvist KC, Tsanov M, Vann SD, Wright NF, Erichsen JT, Aggleton JP, O'Mara SM (2013) The anterior thalamus provides a subcortical circuit supporting memory and spatial navigation. Front Syst Neurosci 7:45.

Jhou TC, Fields HL, Baxter MG, Saper CB, Holland PC (2009) The rostromedial tegmental nucleus (RMTg), a GABAergic afferent to midbrain dopamine neurons, encodes aversive stimuli and inhibits motor responses. Neuron 61:786–800.

Kokel D, Dunn TW, Ahrens MB, Alshut R, Cheung CYJ, Saint-Amant L, Bruni G, Mateus R, van Ham TJ, Shiraki T, Fukada Y, Kojima D, Yeh J-RJ, Mikut R, Lintig von J, Engert F, Peterson RT (2013) Identification of Nonvisual Photomotor Response Cells in the Vertebrate Hindbrain. J Neurosci 33:3834–3843.

Krishnan S, Mathuru AS, Kibat C, Rahman M, Lupton CE, Stewart J, Claridge-Chang A, Yen S-C, Jesuthasan S (2014) The Right Dorsal Habenula Limits Attraction to an

522 Odor in Zebrafish. Curr Biol.

523 Lee A, Mathuru AS, Teh C, Kibat C, Korzh V, Penney TB, Jesuthasan S (2010) The
524 habenula prevents helpless behavior in larval zebrafish. Curr Biol 20:2211–2216.

525 Lee S-H, Dan Y (2012) Neuromodulation of Brain States. Neuron 76:209–222.

526 LeGates TA, Altimus CM, Wang H, Lee H-K, Yang S, Zhao H, Kirkwood A, Weber ET,
527 Hattar S (2012) Aberrant light directly impairs mood and learning through
528 melanopsin-expressing neurons. Nature 491:594–598.

529 Marburg O (1944) The structure and fiber connections of the human habenula. Journal
530 of Comparative Neurology 80:211–233.

531 Marder E (2012) Neuromodulation of neuronal circuits: back to the future. Neuron 76:1–
532 11.

533 Maruyama R, Maeda K, Moroda H, Kato I, Inoue M, Miyakawa H, Aonishi T (2014)
534 Detecting cells using non-negative matrix factorization on calcium imaging data.
535 Neural Networks 55:11–19.

536 Matsumoto M, Hikosaka O (2007) Lateral habenula as a source of negative reward
537 signals in dopamine neurons. Nature 447:1111–1115.

538 Matsumoto M, Hikosaka O (2009) Representation of negative motivational value in the
539 primate lateral habenula. Nat Neurosci 12:77–84.

540 Mitchell AS, Sherman SM, Sommer MA, Mair RG, Vertes RP, Chudasama Y (2014)
541 Advances in Understanding Mechanisms of Thalamic Relays in Cognition and
542 Behavior. Journal of Neuroscience 34:15340–15346.

543 Miyasaka N, Morimoto K, Tsubokawa T, Higashijima S-I, Okamoto H, Yoshihara Y
544 (2009) From the olfactory bulb to higher brain centers: genetic visualization of
545 secondary olfactory pathways in zebrafish. J Neurosci 29:4756–4767.

546 Morley BJ, Spangler KM, Javel E (1985) The development of somatostatin
547 immunoreactivity in the interpeduncular nucleus of the cat. Brain Res 352:241–248.

548 Mueller T (2012) What is the Thalamus in Zebrafish? Front Neurosci 6:64.

549 Newman J (1995) Thalamic contributions to attention and consciousness. Conscious
550 Cogn 4:172–193.

551 Portugues R, Feierstein CE, Engert F, Orger MB (2014) Whole-brain activity maps
552 reveal stereotyped, distributed networks for visuomotor behavior. Neuron 81:1328–
553 1343.

554 Quina LA, Tempest L, Ng L, Harris JA, Ferguson S, Jhou TC, Turner EE (2014) Efferent
555 Pathways of the Mouse Lateral Habenula. J Comp Neurol.

556 Robles E, Laurell E, Baier H (2014) The retinal projectome reveals brain-area-specific
557 visual representations generated by ganglion cell diversity. Curr Biol 24:2085–2096.

558 Romanski LM, LeDoux JE (1992) Equipotentiality of thalamo-amygdala and thalamo-
559 cortico-amygdala circuits in auditory fear conditioning. Journal of Neuroscience
560 12:4501–4509.

561 Satou C, Kimura Y, Hirata H, Suster ML, Kawakami K, Higashijima S-I (2013)
562 Transgenic tools to characterize neuronal properties of discrete populations of
563 zebrafish neurons. Development 140:3927–3931.

564 Semm P, Demaine C (1984) Electrophysiology of the pigeon's habenular nuclei:
565 evidence for pineal connections and input from the visual system. Brain Res Bull
566 12:115–121.

567 Semmelhack JL, Donovan JC, Thiele TR, Kuehn E, Laurell E, Baier H (2014) A
568 dedicated visual pathway for prey detection in larval zebrafish. Elife 3:17968.

569 Sherman SM, Guillery RW (2002) The role of the thalamus in the flow of information to
570 the cortex. Philos Trans R Soc Lond, B, Biol Sci 357:1695–1708.

571 Steenbergen PJ, Richardson MK, Champagne DL (2011) Patterns of avoidance
572 behaviours in the light/dark preference test in young juvenile zebrafish: a
573 pharmacological study. Behav Brain Res 222:15–25.

574 Stephenson-Jones M, Floros O, Robertson B, Grillner S (2012) Evolutionary
575 conservation of the habenular nuclei and their circuitry controlling the dopamine and
576 5-hydroxytryptophan (5-HT) systems. Proc Natl Acad Sci USA 109:E164–E173.

577 Thornton EW, Davies C (1991) A water-maze discrimination learning deficit in the rat
578 following lesion of the habenula. Physiol Behav 49:819–822.

579 Vandewalle G, Schwartz S, Grandjean D, Wuillaume C, Balteau E, Degueldre C,
580 Schabus M, Phillips C, Luxen A, Dijk DJ, Maquet P (2010) Spectral quality of light
581 modulates emotional brain responses in humans. Proceedings of the National
582 Academy of Sciences 107:19549–19554.

583 Walker AS, Burrone J, Meyer MP (2013) Functional imaging in the zebrafish retinotectal
584 system using RGECO. Front Neural Circuits 7.

585 Wang RY, Aghajanian GK (1977) Physiological evidence for habenula as major link

586 between forebrain and midbrain raphe. Science 197:89–91.

587 Ward LM (2013) The thalamus: gateway to the mind. Wiley Interdisciplinary Reviews:
588 Cognitive Science.

589 Wimmer RD, Schmitt LI, Davidson TJ, Nakajima M (2015) Thalamic control of sensory
590 selection in divided attention. Nature.

591 Wyart C, Del Bene F, Warp E, Scott EK, Trauner D, Baier H, Isacoff EY (2009)
592 Optogenetic dissection of a behavioural module in the vertebrate spinal cord. Nature
593 461:407–410.

594 Yañez J, Anadon R (1994) Afferent and efferent connections of the habenula in the
595 larval sea lamprey (Petromyzon marinus L.): an experimental study. J Comp Neurol
596 345:148–160.

597 Zhang J, Tan L, Ren Y, Liang J, Lin R, Feng Q, Zhou J, Hu F, Ren J, Wei C, Yu T,
598 Zhuang Y, Bettler B, Wang F, Luo M (2016) Presynaptic Excitation via GABAB
599 Receptors in Habenula Cholinergic Neurons Regulates Fear Memory Expression.
600 Cell 166:716–728.

601 Zhao H, Rusak B (2005) Circadian firing-rate rhythms and light responses of rat
602 habenular nucleus neurons in vivo and in vitro. Neuroscience 132:519–528.

603 Zhao Y, Araki S, Wu J, Teramoto T, Chang Y-F, Nakano M, Abdelfattah AS, Fujiwara M,
604 Ishihara T, Nagai T, Campbell RE (2011) An expanded palette of genetically
605 encoded Ca^{2+} indicators. Science 333:1888–1891.

Figure legends

Figure 1. The habenula responds to change in irradiance

(A) Dorsal view of a live 7 day-old fish, with GCaMP3 expression in the habenula (arrows) under the control of the *s1011tEt* GAL4 driver. (B) A single two-photon slice through the habenula of the fish in panel A. (C) A yz reconstruction at the point indicated by the yellow line in panel B. The dotted lines indicate imaging planes separated by 10 µm. The yellow line indicates the plane imaged in B. (D) Spatial distribution of major responses in the habenula of one fish. 5 planes are shown here. The colors are coded according to the temporal pattern of response, as indicated in (E). Images were collected at a rate of 1 stack/second, and four pulses of light were delivered for 20 seconds each, with variable inter-stimulus interval. (E) Centers of *k*-means clusters corresponding to colors of pixels in (D). (F) Trajectory of the habenula response in (D-E) is shown in two-dimensional state space, using the first two principal components (PC1 and PC2). The first two principal components explain 79.7% of the total variance. Traces are color-coded according to the wedges in panel E to represent direction in which change in irradiance drives the neural state. In panels E and F, the bold lines correspond to light onset while the dashed lines indicate offset.

Figure 2. Habenula response to irradiance change is reproducible.

(A-C) Semi-automated segmentation of habenula neurons. (D-F) K-means cluster analysis of segmented habenula neuron responses to pulses of blue light in 6 fish. Cells with excitation to light (ON, top) or darkness (OFF, middle), or inhibition to light (Inhibitory, bottom) were seen. Traces show cluster centroids, with shaded regions indicating standard error of the mean. (G) Correlation between activity of cells belonging to ON, OFF and Inhibitory (Inh) clusters shown in panels D-F . In general, the ON and OFF responding cells were uncorrelated (correlation coefficient < 0). (H) Activity

631 traces of cells in ON and OFF clusters that showed high correlation with the other
632 category (381 of 1767 cells). The traces showed that this correlation may be due to OFF
633 cells showing slow decay in fluorescence following light ON. Manual inspection of the
634 traces also did not reveal any that responded reliably to both light ON and OFF. Scale
635 bar = 25 µm. a: anterior; p: posterior.

636 **Figure 3. High-speed imaging identifies the dorsal left neuropil as a site of prominent**
637 **response to irradiance change**

638 (A) Dorsal view of the habenula in a 5 day old *Tg(s1011t:GAL4, UAS:GCaMP3)*
639 fish. (B) Relative change in fluorescence (F/F_0) 250 msec after the start of imaging. The
640 arrowhead indicates the dorsal left neuropil. (C) F/F_0 in five different regions of the
641 habenula. (D-H) Light-evoked calcium change in the habenula of a 5 day old
642 *Tg(s1011t:GAL4, UAS: R-GECO)* fish. (D) Average projection of one 20 second time-
643 lapse, showing habenula neurons. (E) F/F_0 200 msec after light onset. (F) Traces from 8
644 different regions, indicated in panel D. (G) Averaged response from 4 recordings of the
645 same fish, imaged at 50 hz, analyzed using non-negative matrix factorization.
646 Arrowhead indicates the dorsal left neuropil. Pixels are colored according to the traces
647 (NMF components) in (H). (I-K) 200 Hz widefield imaging of an *(elavl3:GCaMP6f)* 5 day
648 old fish at the level of the dorsal habenula. (I) Average projection of the initial 2.475
649 seconds of the timelapse. Relative fluorescence change in the colored regions are
650 shown in panel I. (J) Relative change in GCaMP6f fluorescence 100 milliseconds after
651 the onset of light. Increase is seen in the left habenula (red arrowhead) and in the
652 thalamus (white arrowheads). (K) Region 1, which is the dorsal left neuropil, shows a
653 sharp increase in fluorescence. Region 3 shows gradual decrease. The inset shows a
654 zoom of the first 100 milliseconds. No rise is detected in the right habenula at this time.
655 Scale bar = 25 µm.

656 **Figure 4. The thalamus projection to the habenula**

657 (A) Dorsal view of the forebrain of a *Et(SqKR11)* larva, in which habenula afferents
658 from the entopeduncular nucleus are fluorescently labeled. The dorsal left neuropil
659 (arrow) is weakly labeled. (B) Dorsal view of the habenula of a *Et(SqKR11)* larva,
660 following DiD injection into the dorsal neuropil of the left habenula. The parapineal
661 (arrow) has been retrogradely labeled. Habenula afferents from the entopeduncular
662 nucleus are labeled by the transgene, and shown in red here. (C) 80 μm deeper in the
663 same fish, showing bilateral label in the thalamus (white arrows). A labeled cell in the
664 entopeduncular nucleus is also indicated (yellow arrow). (D) Lateral view of another larva,
665 in which the dorsal left neuropil had been injected with DiD. The retrogradely labeled
666 thalamic neuropil is indicated (white arrow). The entopeduncular nucleus is indicated by
667 the yellow arrow. The inset shows a higher magnification labeled thalamic neuropil. Cell
668 bodies are labeled (white arrowhead). (E) A close up view of the neuropil retrogradely
669 labeled by DiD (cyan), in a fish where retinal ganglion cells had been labeled with DiI
670 (yellow). RGC terminals intermingle with fibers from DiD-labeled cells innervating the
671 neuropil (arrow). The arrowhead indicates a DiD thalamic neuron labeled retrogradely.
672 (F) Dorsal view of another fish with DiI injection (yellow) into the right retina, and DiD
673 (cyan) into the left habenula. The thalamic neuropil is indicated (arrowhead). (G) Dorsal
674 view of a 6-day-old fish, labeled with an anti-vGlut1/2, which marks glutamatergic pre-
675 synapses. There is strong label in the dorsal left neuropil (arrowhead). (H) Dorsal view
676 showing label with an anti-GAD65/67 antibody. Labeled puncta are visible in the dorsal
677 left neuropil (arrowhead). No labeled cell bodies were detected. (I) A *Tg(gad1b:RFP,*
678 *vGlut2:GAL4, UAS:eGFP)* fish, with GABAergic cells indicated in magenta, and
679 glutamatergic cells shown in green. Both cell types can be detected in the thalamus. The
680 arrowhead indicates the region of the thalamus that is labeled in panel D. (J) RFP
681 expression in the thalamus of a *Tg(gad1b:RFP)* fish. Arrowheads indicate neurites

extending to the thalamic neuropil. All panels except (G) are single optical sections. EN: entopeduncular nucleus; Pa: pallium; OT: optic tectum; Hb: habenula; Th: thalamus; fr: fasciculus retroflexus. Scale bar = 25 μm.

Figure 5. The thalamus has non-overlapping responses to increase and decrease in irradiance

Dorsal view of the thalamus (A) and habenula (B) of a fish expressing mCherry (magenta) under the control of the *GAL4s1020t* driver. Cell bodies are labeled in the thalamus (A, white arrowheads). Labelled neurites are visible in the thalamic neuropil (A, yellow arrowheads) and in the habenula neuropils (B, arrowheads). The puncta appear to be secreted fragments of the labeled cells. GCaMP6f (green) is broadly expressed in this fish. (C-H) Six different focal planes, from dorsal to ventral, of a fish expressing GCaMP6s in thalamic neurons. The colors of the pixels represent clusters obtained from *k-means* as shown in (I). Responses are seen in the thalamic neuropil (arrowhead) and in neurons (arrows). (I) Cluster centroids obtained from running *k-means* on data in panels (C-H). (J-K) Color coded activity obtained by registering and performing *k-means* on 4 fish, in the dorsal (J) and ventral (K) thalamus. Colored pixels are a maximum projection and superimposed on an image obtained by averaging the 4 fish. Pixels showing an excitation to light are colored blue and those showing an excitation to darkness are in magenta. (L-O) Thalamic afferents in neuropils in the dorsal (L) and ventral (N) habenula. Pixels in cyan show a calcium increase during light ON and traces are plotted as heatmap in the bottom panel of (M) and (O). Pixels in magenta show an increase during light OFF and their heatmaps are shown in the top panel of (M) and (O). In panels I, M and O, blue light was delivered for 20 seconds, with an inter-stimulus interval of 20 seconds. Light onset is indicated by the solid line, while light offset is indicated by the dashed line. a: anterior; p: posterior; Th: thalamus; rHb: right habenula;

lHb: left habenula. Anterior is to the top in all cases. Scale bar = 25 μm.

Figure 6. Optogenetic stimulation of the thalamus

(A) Expression of ChR2-eYFP in the thalamus (arrowheads) of a 5 day old *Tg(s1020t:GAL4, UAS:ChR2-eYFP, elavl3:GCaMP6f)* fish. (B, C) Activity in the habenula of a ChR2-expressing fish, with (B) and without (C) blue LED stimulation of the thalamus. The images show the maximum projections of F/F_0 images for a 25-second period after blue LED illumination, following subtraction of maximum projections of the period before illumination (i.e difference in activity before and after stimulation). (D-F) Heatmaps showing temporal activity from cells segmented in fish with (D, E) and without (F) ChR2. In D (n = 5 fish) and F (n = 2 fish), blue light pulse was given at the time indicated by the black dashed line. No blue light stimulation was given in E (n = 4 fish). Z-scores were calculated by subtracting each time traces by the total mean and dividing by the standard deviation. (G) Mean amplitude of z-scores before and after optogenetic stimulation. Each square stands for a stimulus trial. Amplitude difference before and after stimulation, mean ± 95% CI: 1 Hz: 0.43 ± 0.56, 2 Hz: 0.72 ± 0.35, 4 Hz: 0.89 ± 0.28 and 8 Hz : 1.05 ± 0.18. Scale bar = 25 μm.

Figure 7. The effect of AF4 lesion on habenula response to irradiance change

(A, B) Dorsal view of an 8-day old *Tg(elavl3:GCaMP6f)* fish, before (A) and after (B) lesion of AF4 (arrowheads in panel A). Pixels are colored according to their activity, as indicated by traces in (C). The prominent AF4 sustained response to blue light (cyan pixels) is reduced after lesion, although some response is still detected in the brain (brown pixels). (D, E) Habenula activity before (D) and after (E) lesion of AF4. Pixels are colored according to the traces in (F). There is a reduction in the sustained response to light, but some activity that was not stimulus-locked was still detected. (G) The habenula after lesion of AF9, with pixels colored according to the traces in panel (H). (I) Number of

732 cells in one plane of the dorsal left habenula that are excited by blue light, following
733 lesion of AF4 (n = 12), or AF7 (n = 2) or AF9 (n = 3), or before lesion (n = 5). Error bars
734 represent 95% CI. a: anterior; p: posterior; Pa: pallium; rHb: right habenula. Images are
735 all single optical sections. Scale bar = 25 µm.

736 **Supplemental Figure 1. Dorsal left habenula lesion affects light-dependent behavior**
737 **and raphe activity.**

738 (A-C) A sequence of frames taken during lesioning of the dorsal left neuropil in a
739 *elavl3:GCaMP6f* fish. The laser caused an increase in intracellular calcium in the left
740 habenula, and eventually led to the formation of a bubble at the lesion site (arrow). (D,
741 E) A minimal projection of a time-lapse of control (D) and lesioned (E) fish, imaged at 15
742 Hz using infra-red illumination. The lesioned fish crossed into the dark side, whereas the
743 control did not. (F) Latency to cross into the dark side (n = 25 fish for each group). The
744 bar indicates median. As the assay was run for 10 minutes, a value of 10 indicates a
745 failure to cross. (G-J) Activity in dorsal raphe in an *elavl3:GCaMP6f* fish, before (G) and
746 after (H) lesioning of the dorsal left neuropil. Pixels are color-coded according to the
747 traces in panel (I). Instead of inhibition (magenta), cells show excitation (green) to
748 increase in irradiance. (J) The effect of lesioning the left dorsal habenula neuropil on
749 raphe response in three different fish. Scale bar = 25 µm.

750 **Movie 1. Response in the habenula to increase in irradiance**

751 Widefield imaging of three different focal planes, 10 µm apart, of a fish expressing
752 GCaMP3 in the habenula. Red represents an increase, whereas blue represents a
753 decrease. Responses can be detected throughout the habenula.

754 **Movie 2. Response dynamics in the habenula, as assessed using R-GECO**

755 Time-lapse of R-GECO fluorescence (F/F0) in the habenula of a 5 day old fish,
756 following onset of illumination. Red represents an increase, whereas blue represents a

757 decrease. An increase in fluorescence was detected first in the neuropil of the left
758 habenula, and then in the cell bodies of habenula neurons. This is a *GAL4s1011t,*
759 *UAS:R-GECO* fish. Anterior is to the left.

760 **Movie 3. Widefield imaging of response to blue light onset**

761 200 Hz recording of a 5 day old fish expressing GCaMP6f under the *elavl3*
762 promoter. Dorsal view; anterior is to the left.

763 **Movie 4. Habenula neurons do not project to the thalamus**

764 3D rendition of habenula projection in a zebrafish larva, visualized by expression of
765 RFP under the *narp* promoter (red) and eGFP under the *brn3a* promoter (green). There
766 is a clear projection to the interpeduncular nucleus (IPN), but not to the thalamus.

767 **Movie 5. GAD65/67 label in a zebrafish larva**

768 z-stack of a s*1011Et:GAL4, UAS:GCaMP3* transgenic fish, after immuno-labelling
769 with an antibody to GAD65/67 (magenta). The stack goes from dorsal to ventral.
770 GAD65/67 label is visible in neuropils of the habenula; puncta can be seen between
771 cells in the lateral regions of the habenula in more ventral planes. GAD65/67 labeled
772 cells are visible in the deep focal planes, but these do not express GCaMP3. The
773 location of GAD65/67 expressing cells correlates with the thalamus. S1011Et drives
774 GAL4 expression in the habenula, medial pallium and anterior-lateral pallium. This is a
775 dorsal view, with anterior to the left.

776 **Movie 6. Z-stack of 6 day old *gad1b:RFP, elavl3:GCaMP6f* fish**

777 GABAergic neurons (magenta) are visible in the thalamus, below the habenula.
778 Anterior is to the left. The stack goes from dorsal to ventral.

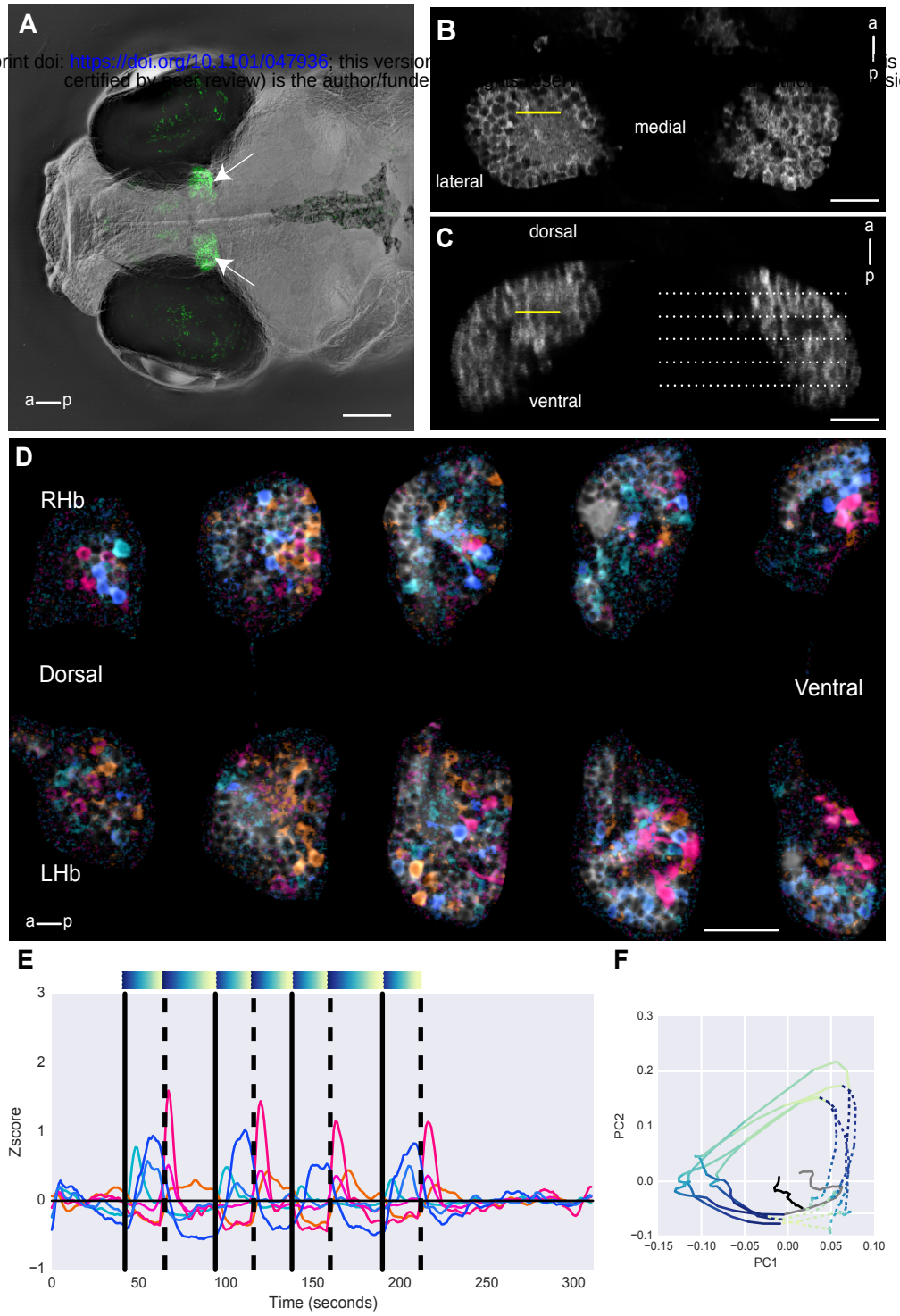

Figure 1. The habenula responds to change in irradiance. (A) Dorsal view of a live 7 day-old fish, with GCaMP3 expression in the habenula (arrows) under the control of the *s1011tEt* GAL4 driver. (B) A single two-photon slice through the habenula of the fish in panel A. (C) A yz reconstruction at the point indicated by the yellow line in panel B. The dotted lines indicate imaging planes separated by 10 µm. The yellow line indicates the plane imaged in B. (D) Spatial distribution of major responses in the habenula of one fish. 5 planes are shown here. The colors are coded according to the temporal pattern of response, as indicated in (E). Images were collected at a rate of 1 stack/second, and four pulses of light were delivered for 20 seconds each, with variable inter-stimulus interval. (E) Centers of *k*-means clusters corresponding to colors of pixels in (D). (F) Trajectory of the habenula response in (D-E) is shown in two-dimensional state space, using the first two principal components (PC1 and PC2). The first two principal components explain 79.7% of the total variance. Traces are color-coded according to the wedges in panel E to represent direction in which change in irradiance drives the neural state. In panels E and F, the bold lines correspond to light onset while the dashed lines indicate offset.

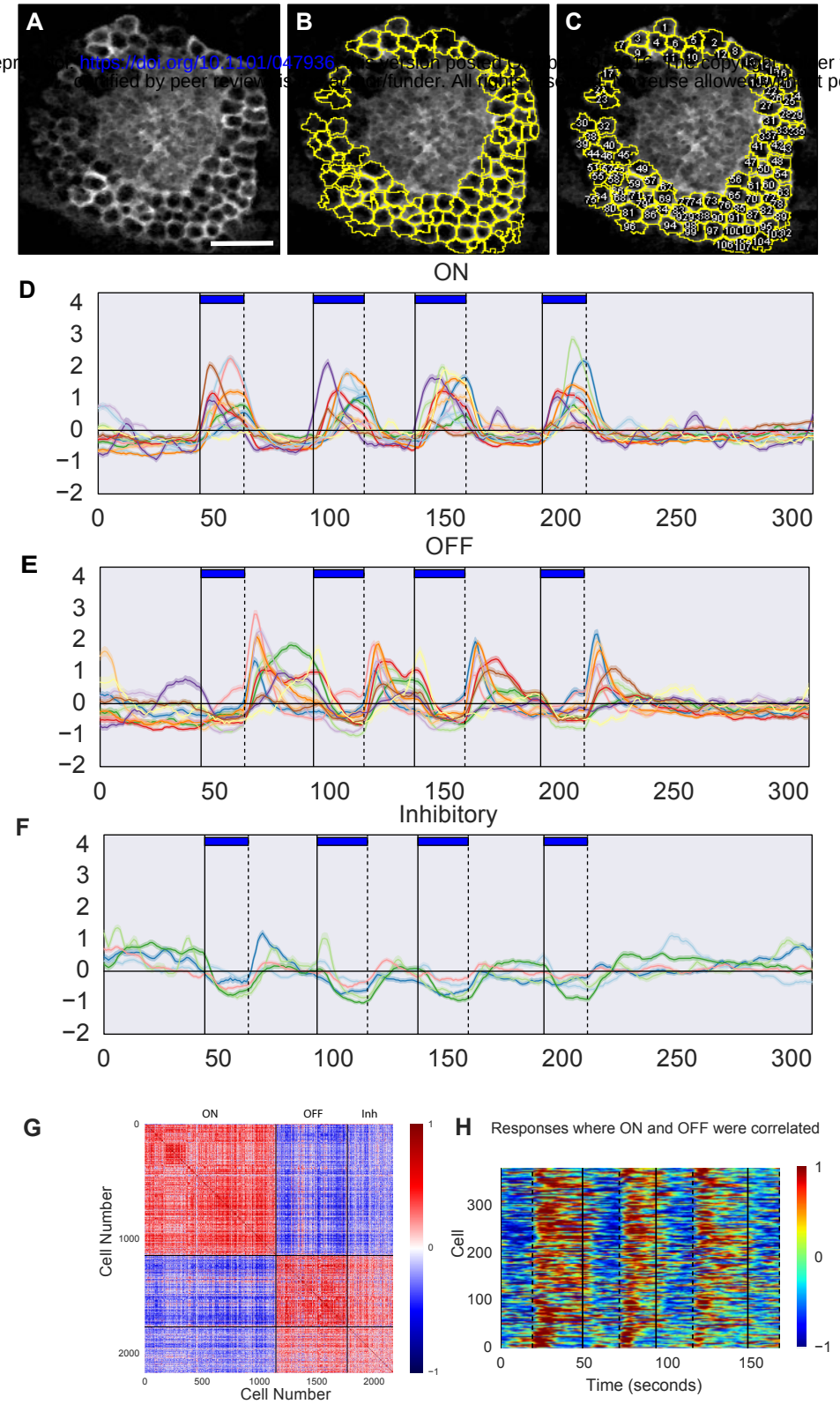

Figure 2. Habenula response to irradiance change is reproducible. (A-C) Semi-automated segmentation of habenula neurons. (D-F) K-means cluster analysis of segmented habenula neuron responses to pulses of blue light in 6 fish. Cells with excitation to light (ON, top) or darkness (OFF, middle), or inhibition to light (Inhibitory, bottom) were seen. Traces show cluster centroids, with shaded regions indicating standard error of the mean. (G) Correlation between activity of cells belonging to ON, OFF and Inhibitory (Inh) clusters shown in panels D-F. In general, the ON and OFF responding cells were uncorrelated (correlation coefficient < 0). (H) Activity traces of cells in ON and OFF clusters that showed high correlation with the other category (381 of 1767 cells). The traces showed that this correlation may be due to OFF cells showing slow decay in fluorescence following light ON. Manual inspection of the traces also did not reveal any that responded reliably to both light ON and OFF. Scale bar = 25 µm.

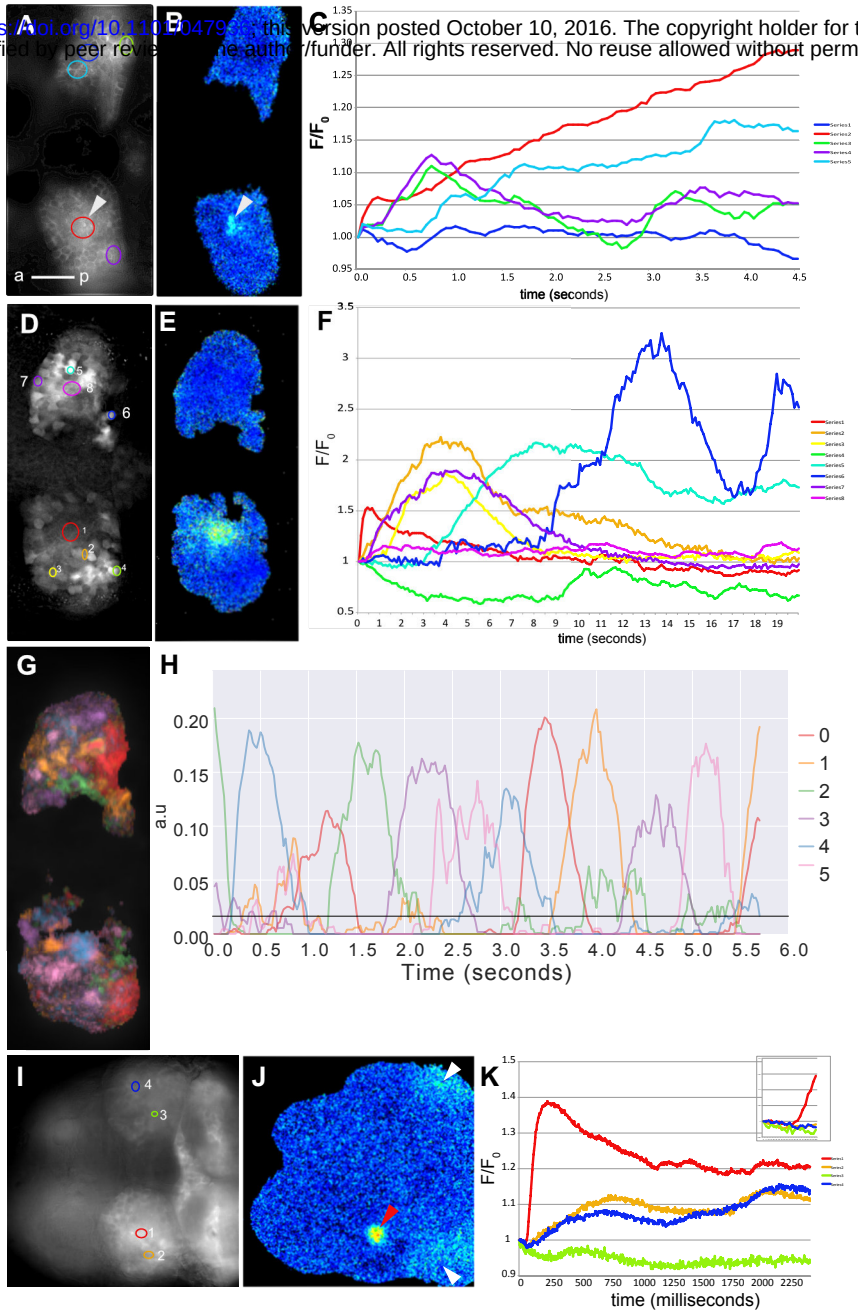

Figure 3. High-speed imaging identifies the dorsal left neuropil as a site of prominent response to irradiance change. (A) Dorsal view of the habenula in a 5 day old *Tg(s1011t:GAL4, UAS:GCaMP3)* fish. (B) Relative change in fluorescence (F/F_0) 250 msec after the start of imaging. The arrowhead indicates the dorsal left neuropil. (C) F/F_0 in five different regions of the habenula. (D-H) Light-evoked calcium change in the habenula of a 5 day old *Tg(s1011t:GAL4, UAS: R-GECO)* fish. (D) Average projection of one 20 second time-lapse, showing habenula neurons. (E) F/F_0 200 msec after light onset. (F) Traces from 8 different regions, indicated in panel D. (G) Averaged response from 4 recordings of the same fish, imaged at 50 hz, analyzed using non-negative matrix factorization. Arrowhead indicates the dorsal left neuropil. Pixels are colored according to the traces (NMF components) in (H). (I-K) 200 Hz widefield imaging of an *(elavl3:GCaMP6f)* 5 day old fish at the level of the dorsal habenula. (I) Average projection of the initial 2.475 seconds of the timelapse. Relative fluorescence change in the colored regions are shown in panel I. (J) Relative change in GCaMP6f fluorescence 100 milliseconds after the onset of light. Increase is seen in the left habenula (red arrowhead) and in the thalamus (white arrowheads). (K) Region 1, which is the dorsal left neuropil, shows a sharp increase in fluorescence. Region 3 shows gradual decrease. The inset shows a zoom of the first 100 milliseconds. No rise is detected in the right habenula at this time. Scale bar = 25 µm.

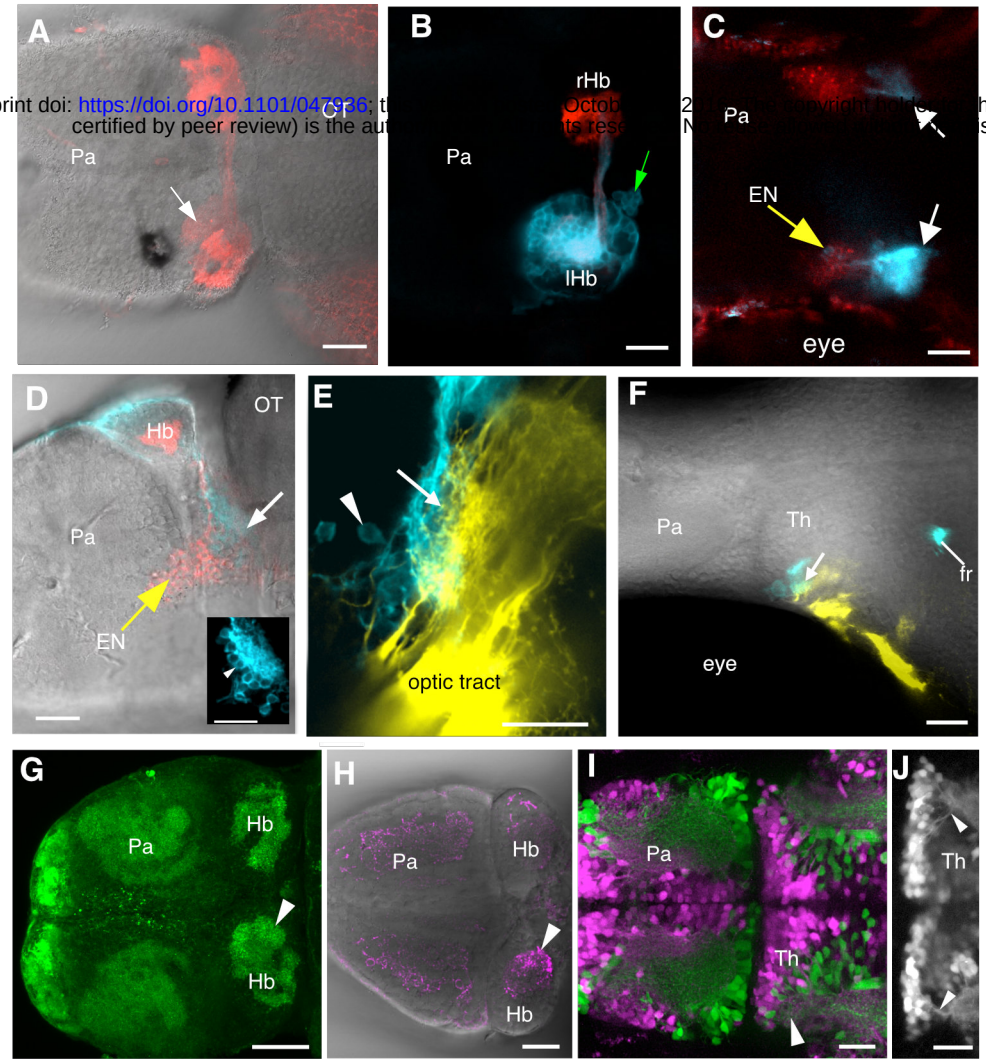

Figure 4. The thalamus projection to the habenula. (A) Dorsal view of the forebrain of a *Et(SqKR11)* larva, in which habenula afferents from the entopeduncular nucleus are fluorescently labeled. The dorsal left neuropil (arrow) is weakly labeled. (B) Dorsal view of the habenula of a *Et(SqKR11)* larva, following DiD injection into the dorsal neuropil of the left habenula. The parapineal (arrow) has been retrogradely labeled. Habenula afferents from the entopeduncular nucleus are labeled by the transgene, and shown in red here. (C) 80 µm deeper in the same fish, showing bilateral label in the thalamus (white arrows). A labeled cell in the entopeduncular nucleus is also indicated (yellow arrow). (D) Lateral view of another larva, in which the dorsal left neuropil had been injected with DiD. The retrogradely labeled thalamic neuropil is indicated (white arrow). The entopeduncular nucleus is indicated by the yellow arrow. The inset shows a higher magnification labeled thalamic neuropil. Cell bodies are labeled (white arrowhead). (E) A close up view of the neuropil retrogradely labeled by DiD (cyan), in a fish where retinal ganglion cells had been labeled with DiI (yellow). RGC terminals intermingle with fibers from DiD-labeled cells innervating the neuropil (arrow). The arrowhead indicates a DiD thalamic neuron labeled retrogradely. (F) Dorsal view of another fish with DiI injection (yellow) into the right retina, and DiD (cyan) into the left habenula. The thalamic neuropil is indicated (arrowhead). (G) Dorsal view of a 6-day-old fish, labeled with an anti-vGlut1/2, which marks glutamatergic pre-synapses. There is strong label in the dorsal left neuropil (arrowhead). (H) Dorsal view showing label with an anti-GAD65/67 antibody. Labeled puncta are visible in the dorsal left neuropil (arrowhead). No labeled cell bodies were detected. (I) A *Tg(gad1b:RFP, vGlut2:GAL4, UAS:eGFP)* fish, with GABAergic cells indicated in magenta, and glutamatergic cells shown in green. Both cell types can be detected in the thalamus. The arrowhead indicates the region of the thalamus that is labeled in panel D. (J) RFP expression in the thalamus of a *Tg(gad1b:RFP)* fish. Arrowheads indicate neurites extending to the thalamic neuropil. All panels except (G) are single optical sections. EN: entopeduncular nucleus; Pa: pallium; OT: optic tectum; Hb: habenula; Th: thalamus; fr: fasciculus retroflexus. Scale bar = 25 µm.

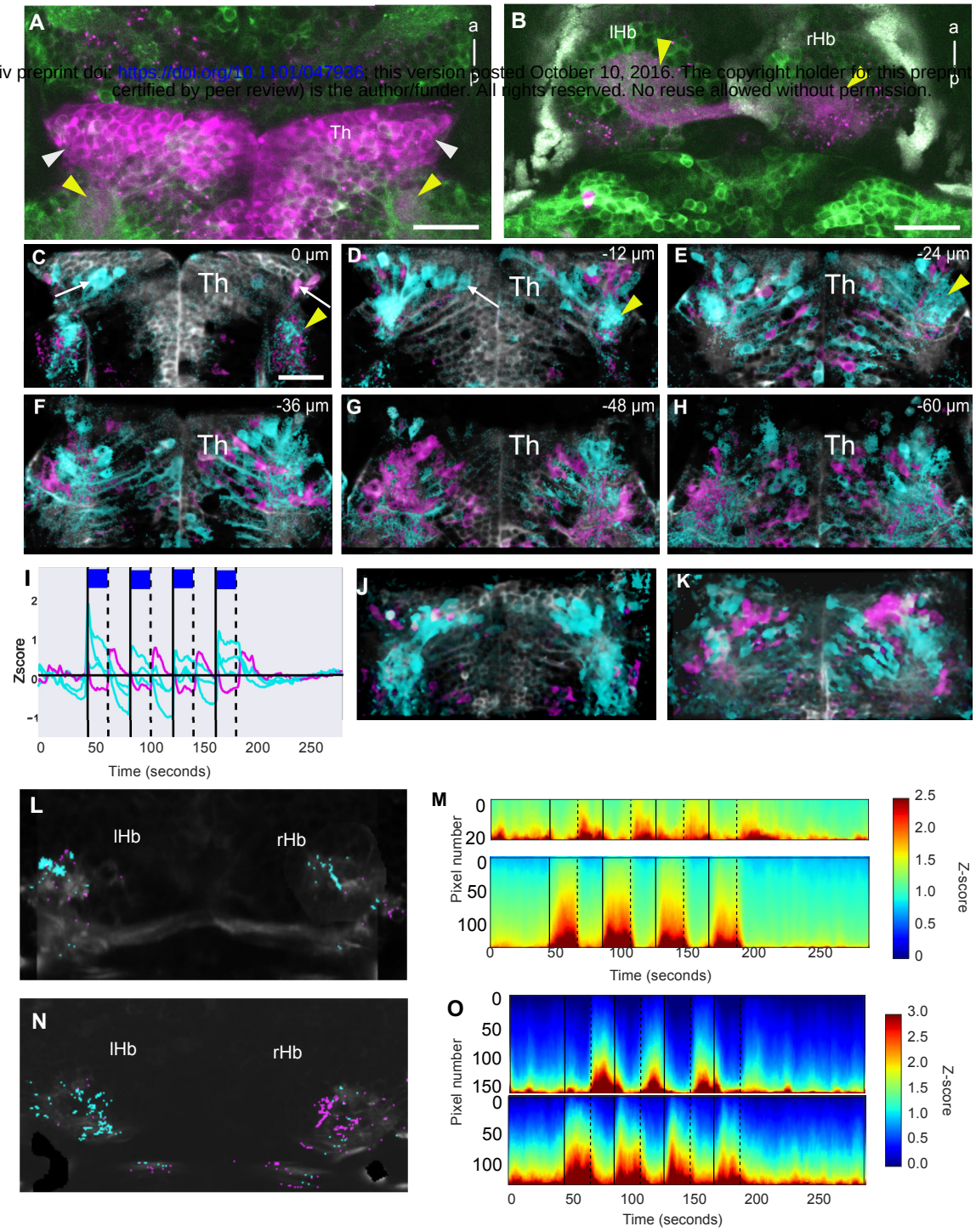

Figure 5. The thalamus has non-overlapping responses to increase and decrease in irradiance. Dorsal view of the thalamus (A) and habenula (B) of a fish expressing mCherry (magenta) under the control of the *GAL4s1020t* driver. Cell bodies are labeled in the thalamus (A, white arrowheads). Labelled neurites are visible in the thalamic neuropil (A, yellow arrowheads) and in the habenula neuropils (B, arrowheads). The puncta appear to be secreted fragments of the labeled cells. GCaMP6f (green) is broadly expressed in this fish. (C-H) Six different focal planes, from dorsal to ventral, of a fish expressing GCaMP6s in thalamic neurons. The colors of the pixels represent clusters obtained from *k-means* as shown in (I). Responses are seen in the thalamic neuropil (arrowhead) and in neurons (arrows). (I) Cluster centroids obtained from running *k-means* on data in panels (C-H). (J-K) Color coded activity obtained by registering and performing *k-means* on 4 fish, in the dorsal (J) and ventral (K) thalamus. Colored pixels are a maximum projection and superimposed on an image obtained by averaging the 4 fish. Pixels showing an excitation to light are colored cyan and those showing an excitation to darkness are in magenta. (L-O) Thalamic afferents in neuropils in the dorsal (L) and ventral (N) habenula. Pixels in cyan show a calcium increase during light ON and traces are plotted as heatmaps in the bottom panel of (M) and (O). Pixels in magenta show an increase during light OFF and their heatmaps are shown in the top panel of (M) and (O). In panels I, M and O, blue light was delivered for 20 seconds, with an inter-stimulus interval of 20 seconds. Light onset is indicated by the solid line, while light offset is indicated by the dashed line. a: anterior; p: posterior; Th: thalamus; rHb: right habenula; lHb: left habenula. Anterior is to the top in all cases. Scale bar = 25 µm.

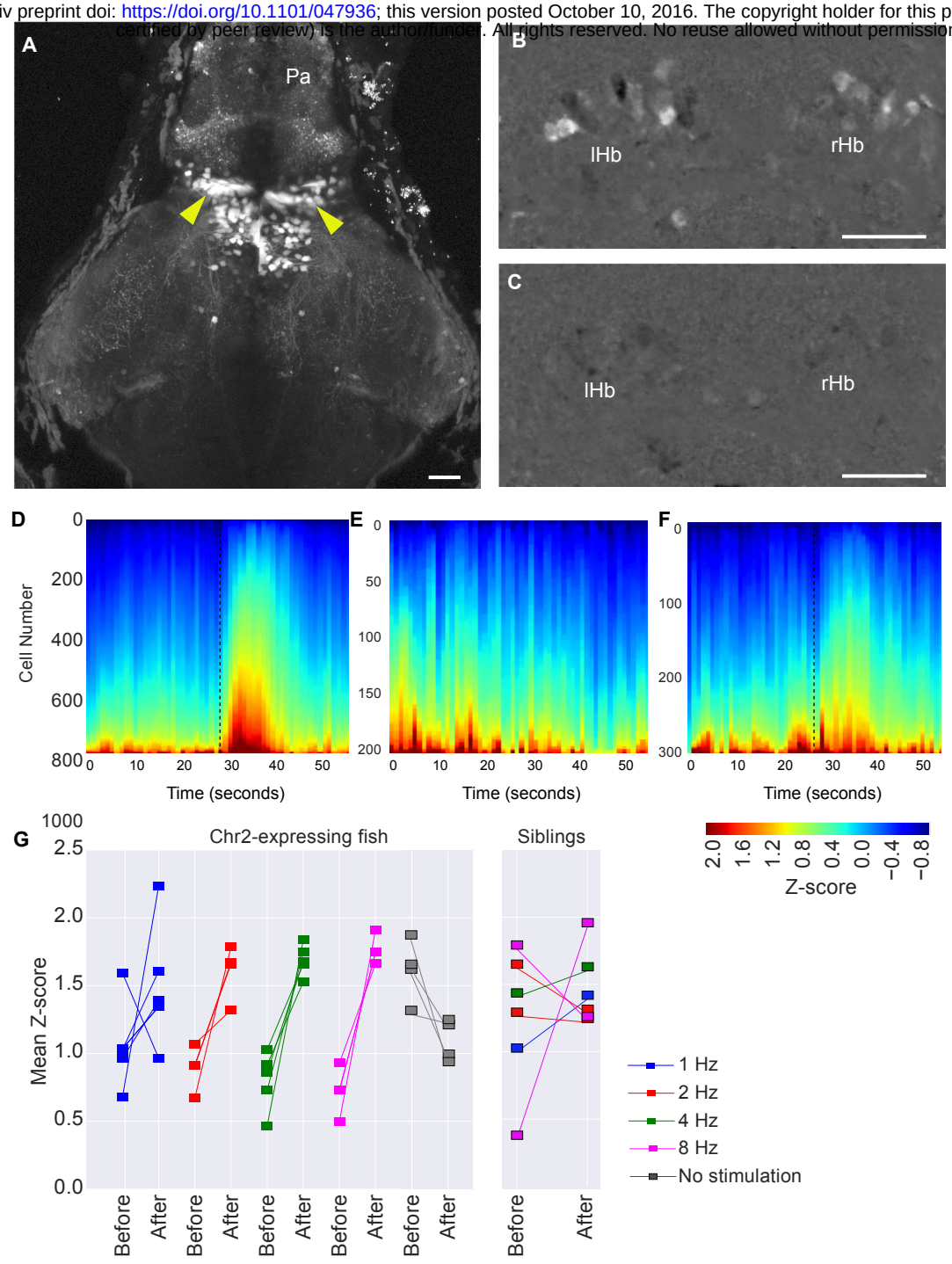

Figure 6. Optogenetic stimulation of the thalamus triggers habenula activity. (A) Expression of ChR2-eYFP in the thalamus (arrowheads) of a 5 day old *Tg(s1020t:GAL4, UAS:ChR2-eYFP, elavl3:GCaMP6f)* fish. (B, C) Activity in the habenula of a ChR2-expressing fish, with (B) and without (C) blue LED stimulation of the thalamus. The images show the maximum projections of F/F_0 images for a 25-second period after blue LED illumination, following subtraction of maximum projections of the period before illumination (i.e difference in activity before and after stimulation). (D-F) Heatmaps showing temporal activity from cells segmented in fish with (D, E) and without (F) ChR2. In D (n = 5 fish) and F (n = 2 fish), blue light pulse was given at the time indicated by the black dashed line. No blue light stimulation was given in E (n = 4 fish). Z-scores were calculated by subtracting each time traces by the total mean and dividing by the standard deviation. (G) Mean amplitude of z-scores before and after optogenetic stimulation. Each square stands for a stimulus trial. Amplitude difference before and after stimulation, mean ± 95% CI: 1 Hz: 0.43 ± 0.56, 2 Hz: 0.72 ± 0.35, 4 Hz: 0.89 ± 0.28 and 8 Hz : 1.05 ± 0.18. Scale bar = 25 µm.

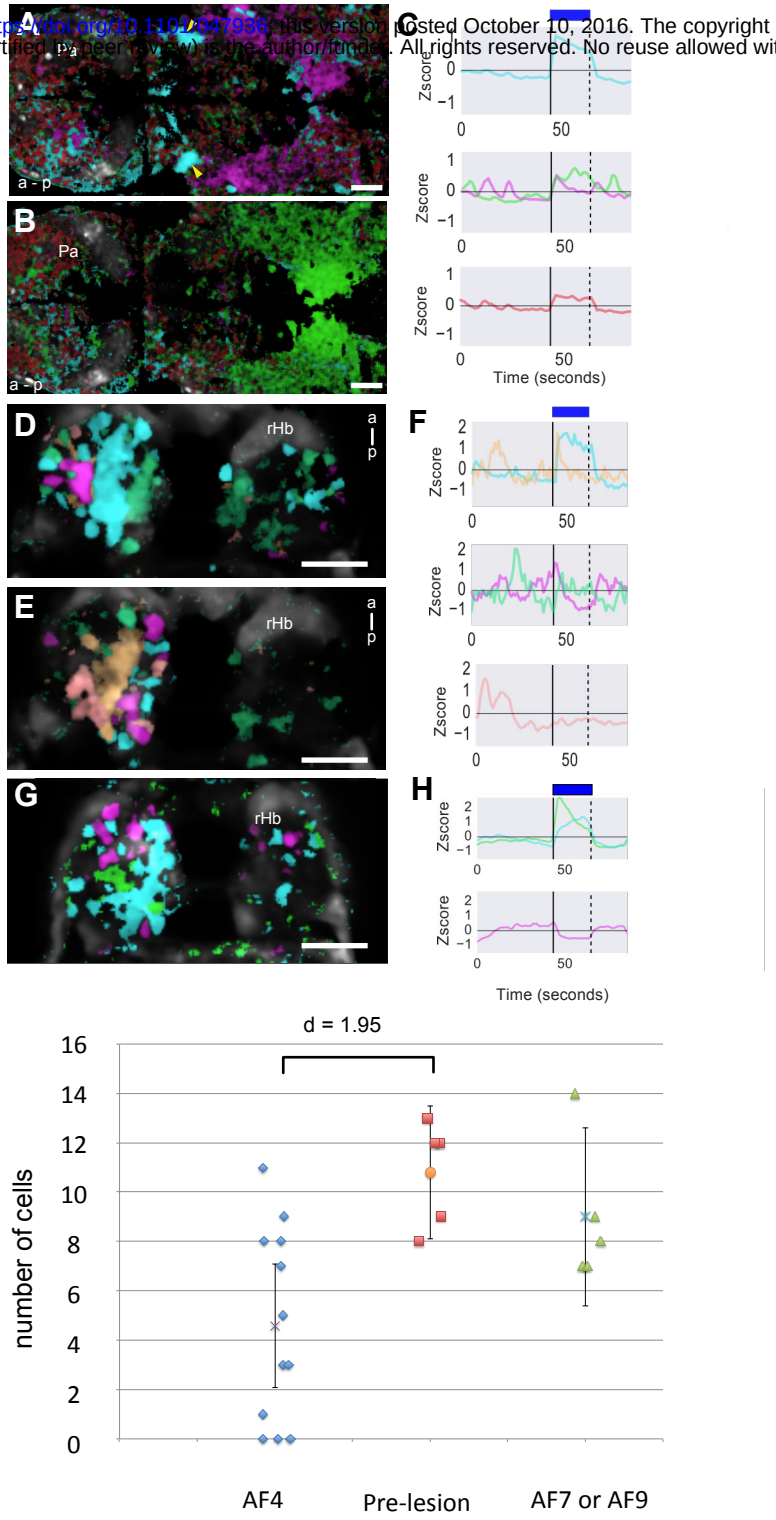

Figure 7. The effect of AF4 lesion on habenula response to irradiance change. (A, B) Dorsal view of an 8-day old Tg(elavl3:GCaMP6f) fish, before (A) and after (B) lesion of AF4 (arrowheads in panel A). Pixels are colored according to their activity, as indicated by traces in (C). The prominent AF4 sustained response to blue light (cyan pixels) is reduced after lesion, although some response is still detected in the brain (brown pixels). (D, E) Habenula activity before (D) and after (E) lesion of AF4. Pixels are colored according to the traces in (F). There is a reduction in the sustained response to light, but some activity that was not stimulus-locked was still detected. (G) The habenula after lesion of AF9, with pixels colored according to the traces in panel (H). (I) Number of cells in one plane of the dorsal left habenula that are excited by blue light, following lesion of AF4 (n = 12), or AF7 (n = 2) or AF9 (n = 3), or before lesion (n = 5). Error bars represent 95% CI. a: anterior; p: posterior; Pa: pallium; rHb: right habenula. Images are all single optical sections. Scale bar = 25 µm.

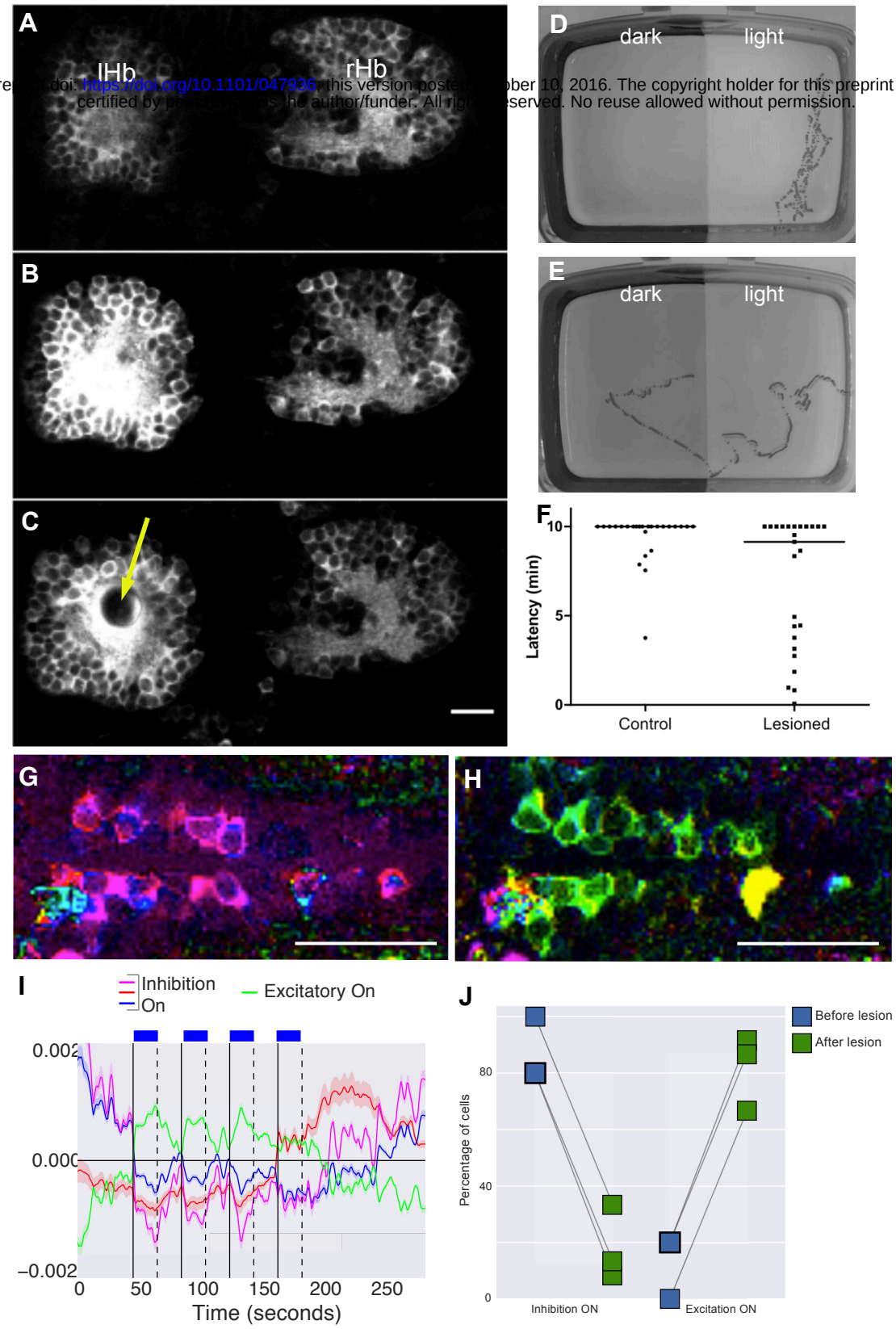

Supplemental Figure 1. Dorsal left habenula lesion affects light-dependent behavior and raphe activity.
(A-C) A sequence of frames taken during lesioning of the dorsal left neuropil in a elavl3:GCaMP6f fish. The laser caused an increase in intracellular calcium in the left habenula, and eventually led to the formation of a bubble at the lesion site (arrow). (D, E) A minimal projection of a time-lapse of control (D) and lesioned (E) fish, imaged at 15 Hz using infra-red illumination. The lesioned fish crossed into the dark side, whereas the control did not. (F) Latency to cross into the dark side (n = 25 fish for each group). The bar indicates median. As the assay was run for 10 minutes, a value of 10 indicates a failure to cross. (G-J) Activity in dorsal raphe in an elavl3:GCaMP6f fish, before (G) and after (H) lesioning of the dorsal left neuropil. Pixels are color-coded according to the traces in panel (I). Instead of inhibition (magenta), cells show excitation (green) to increase in irradiance. (J) The effect of lesioning the left dorsal habenula neuropil on raphe response in three different fish. Scale bar = 25 µm.